

A NEWLY DISCOVERED MOLECULAR CLOUD IN CEPHEUS OB4

JI YANG,¹ YASUO FUKUI, TOMOFUMI UMEMOTO, AND HIDEO OGAWA

Department of Astrophysics, Nagoya University

AND

HUA CHEN

Institute for Astronomy, University of Hawaii

Received 1989 October 2; accepted 1990 April 18

ABSTRACT

A molecular cloud has been discovered from a large-scale ^{13}CO ($J = 1-0$) survey in the Cep OB4 region. Detailed properties of this cloud, named as M120.1+3.0, are investigated on the basis of molecular-line observations and the *IRAS* data. The cloud, appearing dense and filamentary, is composed of two parts. Each of the two parts has a size of $6 \text{ pc} \times 1 \text{ pc}$ and a mass of $800 M_{\odot}$, similar to dark clouds, such as B5, observed within 500 pc of the solar neighborhood. The cloud is associated with ~ 12 low-luminosity ($L \lesssim 20 L_{\odot}$) *IRAS* sources, and the locations of the sources show remarkable coincidence with the distribution of the dense molecular gas. Two molecular outflows have been discovered toward two of the *IRAS* sources. The results indicate that low-mass star formation took place recently in the cloud. Implications of searching for low-mass star-forming clouds at larger distances are discussed.

Subject headings: clusters: associations — infrared: sources — interstellar: molecules — nebulae: H II regions — nebulae: individual (M120.1+3.0) — stars: formation

I. INTRODUCTION

Properties of nearby dark clouds have been extensively studied by many authors (e.g., Myers, Linke, and Benson 1983; Beichman *et al.* 1986). These studies led us to an understanding of typical physical parameters of dark cloud cores and their associated infrared sources, and of the fact that dark clouds are sites of low-mass star formation. A clear tendency in the previous studies is that dark clouds are usually limited within 500 pc from the Sun. For more distant regions, there is no systematic search of such dark clouds, and detailed studies of them are considerably lacking. These kinds of studies are related to the question of low-mass star formation over Galactic scales. Because of larger distances and/or fewer optical and other indicators of these clouds, more efforts are desirable to search for such clouds and to understand star-forming processes within them.

The Cep OB4 complex is one of the star-forming regions located beyond 500 pc from the Sun. Many early-type stars are located within the area outlined by the optical H II region S171. Optical studies indicate the distances to these stars are 850 pc (MacConnell 1968). The H II region was studied previously at optical and low-frequency radio wavelengths by several authors (see Lozinskaya, Sitnik, and Toripova 1987 and references therein). Little is known, however, outside the H II region. An extensive survey of Cep OB4 in ^{13}CO ($J = 1-0$) was thus carried out at Nagoya University in the range from 115° to 125° in Galactic longitude and 0° to 10° in Galactic latitude as part of the all-sky survey at Nagoya University (Fukui 1988, 1989; Fukui *et al.* 1986, 1989, 1990). Three degrees southeast of the giant H II region S171/W1, a filamentary cloud was discovered in this survey. It is located at approximately $l = 120^{\circ}.1$, $b = 3^{\circ}.0$. We designate this cloud as M120.1+3.0.

In this paper, we report molecular-line observations toward

the cloud. The observing methods are described in § II. The observed properties of molecular gas and molecular outflows discovered in the cloud are presented in § IV. The relationships among molecular gas, infrared sources, and molecular outflows are discussed in § V. The conclusions are in § VI.

II. OBSERVATIONS

Observations in ^{12}CO ($J = 1-0$) and its isotopic ^{13}CO ($J = 1-0$) transitions including a large-scale survey were made with the 4 m radio telescope of Nagoya University in several sessions from 1988 December to 1989 May. The half-power beamwidth of the telescope is $2'.7$ at 110 GHz and the beam efficiency is 0.8 (Kawabata *et al.* 1985). A 4 K SIS-mixed receiver gave a typical system temperature of 250 K (DSB). Spectral data were obtained with a 1024 channel acousto-optical spectrometer. The frequency resolution is 40 kHz, corresponding to velocity resolution of 0.11 km s^{-1} at 110 GHz. The total bandwidth is 40 MHz. A room temperature chopper wheel was employed for temperature calibration. Absolute intensity calibration was made by observing S140, and its standard temperatures were taken to be 20 K in ^{12}CO and 6 K in ^{13}CO , respectively. We believe the final results are accurate within 10% after this calibration procedure. Pointing accuracy during the observations was estimated to be better than $20''$.

An outline of the ^{13}CO cloud was first obtained from a quick survey in Cep OB4 region at a grid spacing of $8'$ or $4'$. The cloud area was then fully mapped at a $2'$ grid in ^{13}CO in frequency-switching mode in order to reveal the distribution of dense gas. The region was mapped also in ^{12}CO in two steps for the purpose of searching for outflows. Starting from the coldest infrared sources, we made deep integrations up to 30 minutes toward central positions of 14 *IRAS* sources (see Table 5 below) to achieve high-quality data. In addition, we made an unbiased survey for ^{12}CO wing emission at a grid spacing of $2'$ for the entire ^{13}CO cloud. Integration of 5–10 minutes was achieved for most of the points, with resulting rms noise levels ranging from 0.1 K to 0.2 K (at velocity resolution

¹ Inoue Foundation Fellow, on leave from Purple Mountain Observatory.

TABLE 1
CLOUD PROPERTIES OF M120.1 + 3.0

CLOUD	¹² CO			¹³ CO			Size (pc)
	T_R^* (K)	δV^{12} (km s ⁻¹)	V_{LSR} (km s ⁻¹)	T_R^* (K)	δV^{13} (km s ⁻¹)	V_{LSR} (km s ⁻¹)	
North	10.9	4.3	-19.4	3.5	2.8	-19.4	6.5 × 1.5
South	10.0	3.7	-18.7	2.3	2.4	-17.5	6.6 × 1.9

of 0.11 km s⁻¹). All the ¹²CO spectra were taken in position-switching mode, and only linear base lines were subtracted.

III. DISTANCE

The distance of the cloud is not yet well established at the moment. We will show what constraints we can derive on the distance by using the existing data. On the Palomar Observatory Sky Survey (POSS) prints, the cloud has no sharp boundary although their centers are obviously seen. The cloud has not been listed in any published catalog, the ¹³CO distribution coincides with a few regions of enhanced visual extinction. The intrinsic extinction raised by dust in molecular gas, given the presently observed molecular column densities (see § IV), is around 5 mag using the relation between ¹³CO column density and extinction (see Dickman 1978). This lack of sharp boundary suggests that the cloud is not nearby, i.e., $d \gtrsim 500$ pc. The mean radial velocity of the present cloud, -19 km s⁻¹, is close to the velocities of dense molecular clumps in the central region of the S171 and several other molecular clouds over 10 deg² in the neighborhood of S171 region (Yang and Fukui 1990). In the case of S171, the distance is relatively well determined as 850 pc. Thus, we conclude the cloud is physically related to S171 region, located at a distance of 850 pc.

The distance can also be estimated using the empirical relation by Herbst and Sawyer (1981), which relates the number of

foreground stars counted in 5×5 arcmin², N_* , to the distance of a cloud located within $\pm 20^\circ$ with respect to the Galactic plane and 3 kpc from the Sun by

$$D = 320 N_*^{0.57} \text{ pc} . \quad (1)$$

We counted stars on the POSS prints and have found the mean stellar density N_* in the direction of the north cloud is 5.8. The corresponding distance is 870 pc as estimated by equation (1). This value is well consistent with that of S171. On the other hand, the kinematic distance of the region is estimated as 1.4 kpc from the Galactic rotation model using the ¹³CO radial velocity

$$V_{LSR} = AD \sin(2l) \cos^2(b) \text{ km s}^{-1} , \quad (2)$$

where the distance D is in kpc, l and b are the Galactic longitude and latitude of the cloud, and the Oort constant A was adopted as 15 km s⁻¹ kpc⁻¹. Remembering that the kinetic distance is easily affected by the random motion of clouds, we assume that the cloud is located at the same distance as S171 throughout this paper.

We note that, over all the surveyed region, there is a weak component between -5 km s⁻¹ and 5 km s⁻¹ in V_{LSR} . This component is thought to originate from the Lindblad ring (Dame *et al.* 1987).

IV. RESULTS

a) ¹³CO Results

The gas distribution is inferred from the ¹³CO integrated intensity map in Figure 1. The dense part of the molecular material shows an obvious filamentary structure. The cloud is composed of two parts which are denoted as the *north* and *south* clouds, respectively, in this paper.

The north cloud is elongated in a direction parallel to the Galactic plane. The linear size is ~ 6.5 pc \times 1.5 pc at FWHM level of ¹³CO integrated intensity. Basic parameters of the cloud are listed in Tables 1 and 2. The excitation temperature, T_{ex} , and the optical depth, τ , are derived under the assumption of LTE. These quantities are related to peak radiation temperature T_R^* by

$$T_R^* = [J_\nu(T_{ex}) - J_\nu(T_{bg})](1 - e^{-\tau}) \text{ K} , \quad (3)$$

where $J_\nu(T) = (h\nu/k)/[\exp(h\nu/kT) - 1]$, $T_{bg} = 2.7$ K. The solar abundance ratio of $[X(^{12}\text{CO})/X(^{13}\text{CO})]$, 89, was adopted in deriving the ¹³CO optical depths. The ¹³CO column density,

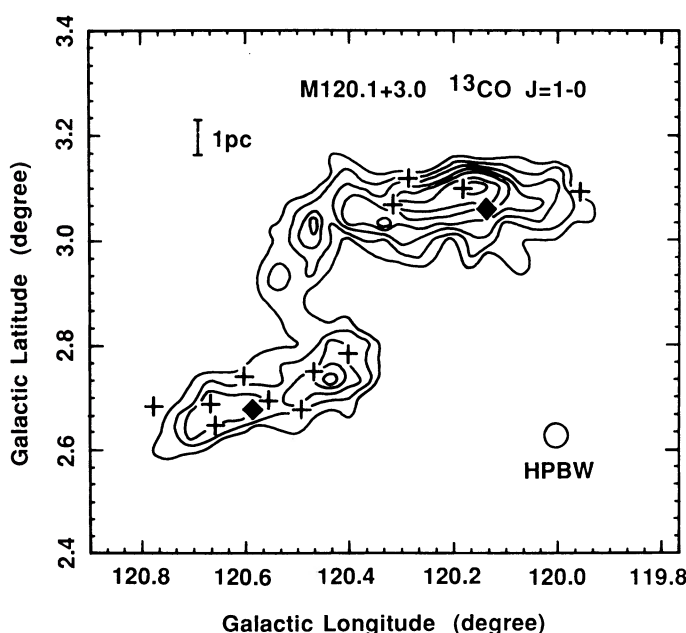


FIG. 1.—A ¹³CO integrated intensity map of M120.1 + 3.0 shown in Galactic coordinates. Contours start from 3.0 K km s⁻¹ with increments of 1.0 K km s⁻¹. IRAS sources within the clouds are marked by crosses, except two of them, 00213 + 6530 and 00259 + 6510, which are labeled by diamonds.

TABLE 2

DERIVED PROPERTIES OF M120.1 + 3.0

Cloud	T_{ex} (K)	τ^{13}	N_{13} ($\times 10^{15}$ cm ⁻²)	M_{cloud} (M_\odot)
North	14.3	0.38	12.8	890
South	13.5	0.26	6.60	610

N^{13} , is related to the peak optical depth and excitation temperature by

$$N^{13} = 2.42 \times 10^{14} T_{\text{ex}} [1 - \exp(-h\nu/kT_{\text{ex}})]^{-1} \tau \Delta\nu \text{ cm}^{-2}, \quad (4)$$

where $\Delta\nu$ is the ^{13}CO line width in km s^{-1} . The abundance ratio $[X(\text{H}_2)/X(^{13}\text{CO})]$ was assumed to be 5×10^5 (Dickman 1978) in deriving the H_2 column density. The H_2 column density at the peak position of the north cloud is $6.4 \times 10^{21} \text{ cm}^{-2}$. The mass of this cloud is estimated to be $890 M_{\odot}$. The volume density can be estimated to be $1.4 \times 10^3 \text{ cm}^{-3}$ by assuming that the path length along the line of sight is the same as the transverse length of the cloud.

The south cloud is tilted to the Galactic plane but also elongated and extended to ~ 6.6 pc long and 1.9 pc wide. Basic parameters are listed in Tables 1 and 2. The mass of this cloud is $610 M_{\odot}$. The peak molecular column density of the south cloud is the half of the north cloud. Both the north and south clouds are linked by a less intense ridge and are supposed to be physically related, since the difference of ^{13}CO radial velocities of the two parts, 1.9 km s^{-1} , is small, clearly less than their ^{13}CO line widths (see Table 1).

The present estimate, which uses only the $J = 1-0$ data, may not adequately take into account possible non-LTE effects. These effects would introduce significant error in mass estimate particularly if the cloud has a nonuniform temperature distribution. To estimate the range of uncertainty in the present LTE hypothesis, we refer the results of a nearby dark cloud B5, which has been studied in detail via both LTE and LVG methods (Young *et al.* 1982; Langer *et al.* 1989). Parameters describing current clouds, such as sizes, masses, and temperature, are similar to those of B5. Both clouds contain only low-luminosity infrared sources (see Table 5 below) which have small influence to the thermal structure of the clouds. For B5, previous studies by employing both the $J = 2-1$ and $1-0$ transitions of ^{12}CO and ^{13}CO show that excitation condition is rather uniform except at the cloud edge. Under such cloud conditions, ^{13}CO traces well the gas distribution (Langer *et al.* 1989). The ^{13}CO cloud mass is $800-930 M_{\odot}$ estimated from LTE, while the LVG analyses give $1200 M_{\odot}$ (Young *et al.* 1982). Results derived from different ways agree within 30%. By comparing the results from the simple LVG analysis for spherical, isothermal, and radially collapsing models and LTE values expected from these models, Dickman (1978) shows that, for column densities derived near the center of these model clouds (corresponding to a reasonable range of A_v), the true values and LTE values are consistent within 35%. We infer the error of LTE column densities derived from current clouds are within the same range, since the both clouds have reasonably similar physical conditions.

A large-scale velocity gradient in the north cloud is apparent in the ^{13}CO data. A position-velocity diagram along the major elongation of the north cloud is shown in Figure 2. The velocity gradient is $\sim 0.3 \text{ km s}^{-1} \text{ pc}^{-1}$. Similar velocity gradients are frequently measured toward nearby dark clouds (Goldsmith and Arquilla 1985). The origin of velocity gradients involved in those dark clouds are interpreted as due to cloud rotation. If the cloud is rotating, the rotational axis is likely to be perpendicular to the Galactic plane, with a rotational period of $\sim 2 \times 10^7$ yr.

b) Mapping of Two Outflows

Two molecular outflows have been discovered in the ^{12}CO survey. One is located in the north cloud and the other in the

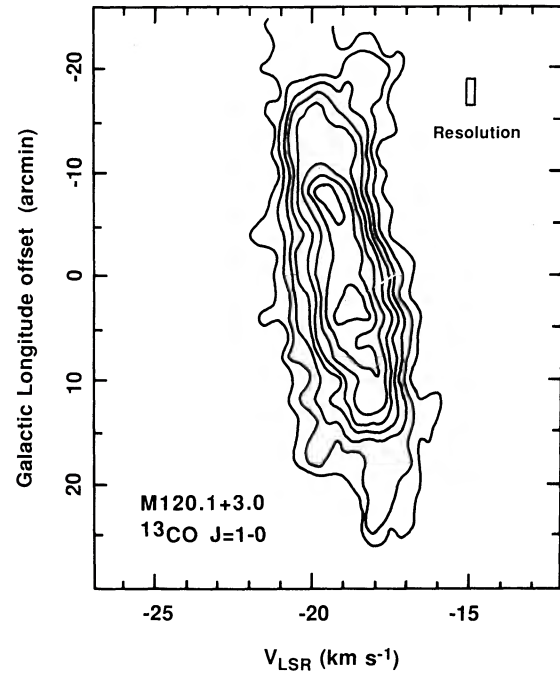


FIG. 2.—A position velocity diagram along a constant Galactic latitude in the north cloud. The lowest contour and the increments are 0.3 K. Center position is $l = 120^{\circ}25$, $b = 3^{\circ}03$.

south cloud. Toward the *IRAS* source, 00259 + 6510, in the south cloud, broad wings have been clearly revealed. Figure 3 shows both ^{12}CO and ^{13}CO spectra taken in the direction of this *IRAS* point source. The total velocity extent of the ^{12}CO high-velocity wings was measured to be greater than $\sim 14.7 \text{ km s}^{-1}$ at the 0.1 K level. At the extreme red side, the wing component is probably contaminated by foreground emission. A contour map of ^{12}CO wing components are shown in Figure 4. The source, 00259 + 6510, is marked by a cross. Both velocity components are localized and the red wing is more intense than the blue one.

Wing components were also discovered around 00213 + 6130 in the north cloud. Spectra of ^{12}CO and ^{13}CO transitions toward the *IRAS* source and a contour map of

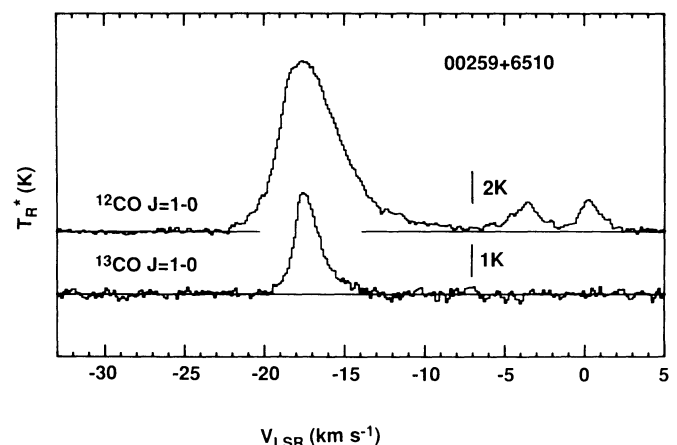


FIG. 3.—Spectra of ^{12}CO ($J = 1-0$) and ^{13}CO ($J = 1-0$) taken in the direction of *IRAS* 00259 + 6510. The position of $\alpha(1950) = 0^{\text{h}}25^{\text{m}}59^{\text{s}}.8$, $\delta = 65^{\circ}10'11''$. A weak foreground component at $V_{\text{LSR}} = -3 \text{ km s}^{-1}$ is visible.

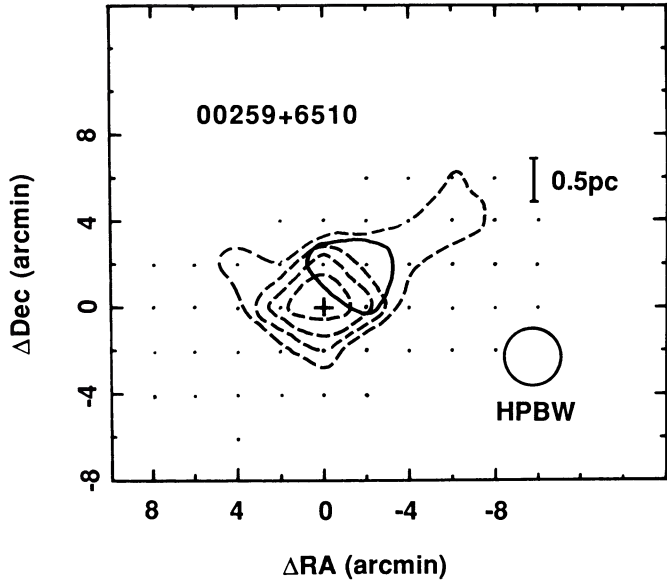


FIG. 4.—A ^{12}CO contour map of wing components in the direction of 00259 + 6510. Dashed lines denote the intensity integrated from -14.0 km s^{-1} to -7.5 km s^{-1} . Solid lines represent the intensity from -25.0 km s^{-1} to -21.0 km s^{-1} . Contours start from 2.0 K km s^{-1} with increments of 1.0 K km s^{-1} . The suggested driving source, 00259 + 6510, is denoted by a cross. Observed points are marked by dots.

high-velocity emission are presented in Figures 5 and 6, respectively. The wing emission extends over 18 km s^{-1} at the 0.1 K level. The intensity of the wing emission of this source is weaker than that of 00259 + 6510. Both the geometric location and the cold IR color favor that 00213 + 6530 is the driving source of the outflow.

Observed parameters of the outflows and their ambient gas are listed in Table 3. Columns (2) and (3) are ^{12}CO radiation temperatures and radial velocities of two sources. Column (4) is the velocity range of the ^{12}CO red wings, and column (5) is their integrated intensities. Column (6) contains the areas of the red wings measured at half maximum levels. From columns (7)–(9) are corresponding quantities for blue wings. Molecular column densities of flow gas were calculated from ^{12}CO data under the assumption of LTE,

$$N^{12} = 4.2 \times 10^{13} T_{\text{ex}} \exp(hv/kT_{\text{ex}}) \times [\tau/(1 - \exp(-\tau))] \int T_R^*(v) dv \text{ cm}^{-2}, \quad (5)$$

where τ is the mean ^{12}CO optical depth over the velocity range in the integration and $\int T_R^*(v) dv$ is in K km s^{-1} . The integrations were evaluated in the velocity ranges listed in columns (4) and (7) in Table 3 for each component. There are very few works on the density of outflow sources (e.g., Phillips *et al.*

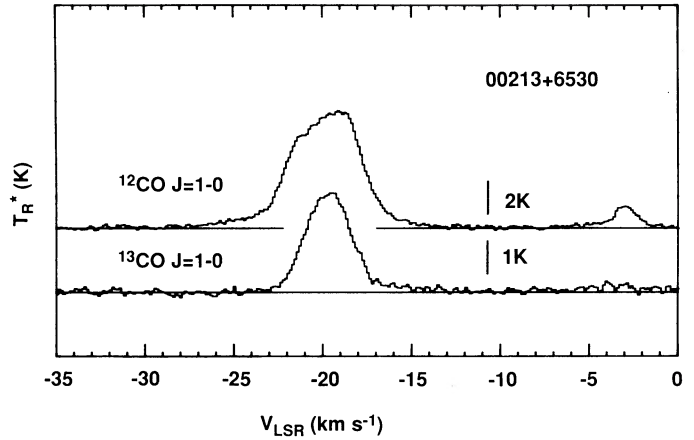


FIG. 5.—Spectra of ^{12}CO ($J = 1-0$) and ^{13}CO ($J = 1-0$) taken at $\alpha(1950) = 0^{\circ}21'22.0''$, $\delta = 65^{\circ}30'25''$ of 00213 + 6530 in the north cloud. Weak foreground components at $V_{\text{LSR}} = 0$ and -4 km s^{-1} are present.

1988). The results show that the densities of outflow gas are usually within 10^{3-5} cm^{-3} . In such density ranges, the ^{12}CO and ^{13}CO excitation temperature is likely similar. Assuming that the excitation temperature of outflow gas is close to that of the ambient gas (Snell *et al.* 1984), we derived physical param-

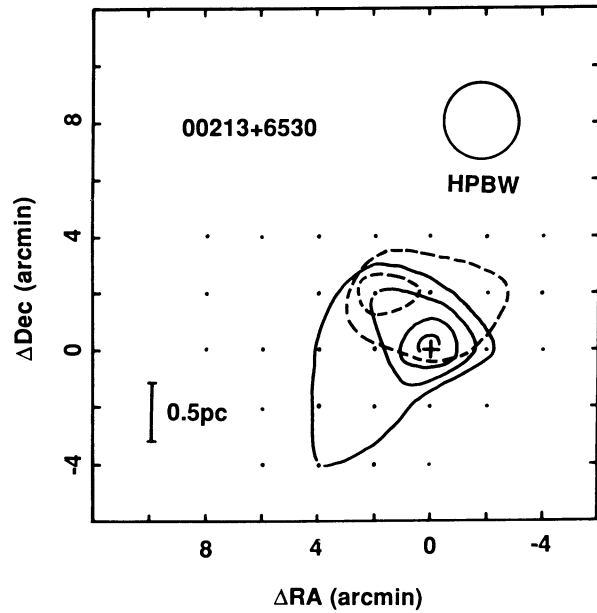


FIG. 6.—A contour map of wing components in 00213 + 6530 direction. Contours start from 1.0 K km s^{-1} with increments of 0.5 K km s^{-1} . The source 00213 + 6530 is denoted by a cross in the center. Observed points are denoted by dots. Dashed lines denote integration from -16.6 km s^{-1} to -13.4 km s^{-1} . Solid lines are from -27.8 km s^{-1} to -22.8 km s^{-1} .

TABLE 3
OBSERVED PARAMETERS OF OUTFLOWS

OBJECT (1)	T_R^* (K) (2)	V_{LSR} (km s^{-1}) (3)	RED			BLUE		
			V_{red} (km s^{-1}) (4)	$\int T_R^* dv$ (K km s^{-1}) (5)	A_w ($\text{pc} \times \text{pc}$) (6)	V_{blue} (km s^{-1}) (7)	$\int T_R^* dv$ (K km s^{-1}) (8)	A_w ($\text{pc} \times \text{pc}$) (9)
00213 + 6530.....	7.5	-19.9	(-16.6 to -13.4)	1.8	1.7×1.0	(-27.8 to -22.8)	2.7	1.7×1.0
00259 + 6510.....	10.7	-17.3	(-14.0 to -7.5)	5.4	1.2×1.0	(-25.0 to -21.0)	2.3	1.0×1.0

TABLE 4
ENERGETICS OF OUTFLOWS

Object (1)	Wing (2)	V_{range} (km s^{-1}) (3)	Age ($\times 10^5$ yr) (4)	N_{12} ($\times 10^{15} \text{ cm}^{-2}$) (5)	Mass (M_{\odot}) (6)	MV ($M_{\odot} \text{ km s}^{-1}$) (7)	$MV^2/2$ ($\times 10^{44}$ ergs) (8)	$MV^3/2R$ ($\times 10^{-2} L_{\odot}$) (9)
00213+6530.....	Red	6.50	1.97	3.45	0.46	2.94	1.90	0.80
	Blue	7.90	1.62	5.16	0.67	5.37	4.21	2.14
00259+6510.....	Red	9.80	1.07	12.3	1.13	11.1	10.8	8.42
	Blue	7.70	1.23	5.92	0.39	3.10	2.38	1.59

eters at the center position of each outflow (referring col. [2] in Table 2).

The optical depth of outflow gas should be estimated before equation (5) is calculated. Limited by the fact that, over most of the ^{12}CO wing velocity range, the corresponding ^{13}CO wing emission is weak and below the noise level, it is impossible to derive ^{12}CO optical depth directly. We thus adopted the following approach. The optical depths of the inner-most ^{13}CO wings were calculated to estimate the possible range of the ^{12}CO optical depths of the outflow gas. In the case of 00259+6510, the ^{13}CO optical depth is 0.05 for the inner-most red ($v = -15.0$ to -14.0 km s^{-1}) wing component. The ^{12}CO optical depth is 4, adopting $[X(^{12}\text{CO})/X(^{13}\text{CO})]$ to be 89. For outer velocity ranges, the ^{12}CO optical depth is expected to decrease and finally vanish (e.g., Plambeck, Snell, and Loren 1983). We therefore simply adopt the mean ^{12}CO optical depth of 2 for equation (5). The possible range of error of τ involved in such an approximate way is expected to be within a factor of 2, and the related error of column density is within a factor of 2.3.

Masses of outflow components were derived from ^{12}CO column densities using

$$M = 9.83 \times 10^{-17} A_w N^{12} M_{\odot}, \quad (6)$$

where A_w , in unit of pc^2 , is the area of the flow components listed in Table 3. The derived masses, momenta, and kinetic energies are listed in columns (6)–(8) in Table 4. These values are typical of outflows discovered in dark clouds (e.g., Goldsmith *et al.* 1984).

The dynamic ages of the two outflows were estimated from the separation between the two FWHM contours of the wing emissions, divided by the maximum velocity extents measured at the position of the driving source. Ages derived from red and blue wings are quite similar for both objects. The resultant values are listed in column (3) of Table 4. These values are larger than 1×10^5 yr, indicating that the two sources are relatively old. Column (9) in Table 4 contains mechanical luminosities calculated from the dynamic ages and kinetic energies.

V. DISCUSSION

a) Low-Mass Star Formation within Clouds

Fourteen *IRAS* sources are located inside the ^{13}CO mapped region, as cataloged in the *IRAS Point Source Catalog* (1988), although the fluxes are generally lower limits. The co-added data are thus used here for discussion.

The fluxes of the sources were determined by the ADDSCAN process at the IPAC. At each given source position, 10–12 single scans in the in-scan direction were extracted from the *IRAS* data base, and were co-added to construct the ADDSCAN. Sixteen flux estimators were produced from the ADDSCAN in each wave band. Each flux was then determined by selecting one of the 16 estimators according to the source intensity profile, source extent, baseline fitting, and the point source template fitting. The resulted fluxes and related rms levels are listed in columns (5)–(12) in Table 5. Fluxes larger than 3 times of the rms values are given in the table, resulted the detection at more wave bands. The sensitivity has been

TABLE 5
IRAS SOURCES IN M120.1+3.0

Number ^a (1)	<i>IRAS</i> Name (2)	R.A.(1950) (3)	Decl.(1950) (4)	F_{12}^b (5)	σ_{12} (6)	F_{25} (7)	σ_{25} (8)	F_{60} (9)	σ_{60} (10)	F_{100} (11)	σ_{100} (12)	L_{IRAS}^c (13)	Note ^d (14)
1	00196+6531	0 ^h 19 ^m 36 ^s .5	65°31'09"	0.28	0.024	...	0.016	...	0.239	...	2.541	1.2	S
2	00213+6530	0 21 22.0	65 30 24	0.20	0.029	0.95	0.033	4.64	0.052	16.46	1.095	12.9	O
3	00217+6533	0 21 45.6	65 33 00	0.16	0.039	0.74	0.031	3.95	1.000	17.29	4.000	12.0	
4	00227+6534	0 22 44.5	65 34 49	0.15	0.034	0.39	0.031	2.43	0.283	18.00	5.000	10.2	
5	00230+6532	0 23 4.5	65 32 02	...	0.042	...	0.030	4.00	0.080	14.62	0.803	(9.2)	
6	00241+6515	0 24 9.9	65 15 33	...	0.043	0.72	0.049	2.25	0.247	...	3.000	3.3	
7	00248+6513	0 24 49.2	65 13 54	0.76	0.038	1.79	0.156	5.97	0.555	10.08	1.235	15.6	C
8	00251+6509	0 25 6.6	65 09 38	1.42	0.025	0.39	0.061	...	0.216	...	0.485	6.8	S
9	00256+6511	0 25 41.2	65 11 03	0.55	0.053	1.20	0.101	9.51	0.223	18.63	0.623	20.3	
10	00259+6510	0 25 59.8	65 10 11	0.67	0.049	1.99	0.063	4.00	1.000	...	5.000	9.9	O
11	00260+6514	0 26 5.9	65 14 01	0.64	0.065	...	0.091	...	0.363	...	1.105	2.8	S
12	00266+6508	0 26 41.6	65 08 43	0.30	0.046	1.00	0.058	6.60	0.160	17.20	1.131	15.6	
13	00267+6511	0 26 44.9	65 11 15	0.39	0.029	1.03	0.032	8.17	0.203	18.36	1.819	17.9	C
14	00277+6511	0 27 47.3	65 11 31	0.56	0.034	0.81	0.030	1.00	0.234	3.75	0.943	(6.1)	

^a NOTES ON INDIVIDUAL SOURCE: 1, hot source; 2, good point source, but confused in 100 μm ; 3, double sources in 12, 25 μm , but confused in 60, 100 μm ; 4, extended source; 5, cold, confused in 100 μm ; 6, confused in 100 μm ; 7, good point source; 8, hot point source; 9, several sources in the field in 12, 25 μm , but they are confused in 60, 100 μm ; 10, rather hot, confused in 60 and 100 μm ; 11, hot; 12, extended; 13, good data, may be extended; 14, confused.

^b Fluxes and errors in units of Jy.

^c Luminosity in unit of L_{\odot} .

^d S: visible star; O: outflow; C: outflow candidate.

significantly improved by a factor of 3. Comparison of the co-added fluxes with the values carried in the Point Source Catalog shows rather good consistency between the two sets of data.

The two sources, 00196+6531 and 00260+6514, are detected only at 12 μm band. The color properties of these sources indicate they are hot in nature. Another source, 00251+6509, detected at 12 and 25 μm , also shows hot color. Each of them is probably associated with a visible star, as identified in the *IRAS* catalog. These stars are also recognizable in the POSS prints.

Color temperature derived from fluxes in the 12 and 25 μm bands ranges from 120 to 380 K assuming the dust emissivity law $\kappa_\nu \sim \nu^1$, indicating that the cloud is associated with both cold and hot sources. The source 00230+6532 is detected at 60 and 100 μm bands but confused at 100 μm . This source is cirrus-like (Beichman 1986). The source 00277+6511 is also confused, and its properties are difficult to access. These two sources may not be self-illuminating and are excluded from following discussion. The driving source of the outflow in the north cloud, 00213+6530, shows characteristics of a good point source. The driving source of the outflow in the south cloud, 00259+6510, is relatively hot and confused in 60 and 100 μm . Another two sources, 00248+6513 and 00267+6511, exhibit good data qualities. Color properties of these sources suggest these sources are embedded (Emerson 1987).

An interesting feature is that the distribution of the *IRAS* sources distinctly delineates the dense molecular gas, suggesting that at least part of them must be in real association with the clouds (see Fig. 1). The association of molecular outflows with two of these sources provides direct evidence for that these sources represent newly formed young stellar objects which are still embedded inside dense molecular gas. It is possible that compact outflows are missing as a result of the current beam size (~ 0.7 pc at the cloud distance), which makes any discussion of the dynamical influence on the outflows on the ambient matter incomplete. In fact, the sources, 00248+6513 and 00267+6511, are outflow candidates which exhibit broad wing components but could not be resolved under the beam size. Nevertheless, the current detection rate of outflow sources, $\sim 20\%$, is close to that found in opaque dark clouds (Frerking and Langer 1982), or in HH objects (Edwards and Snell 1984). A higher spatial resolution survey combined with improved sensitivity will probably reveal more outflow sources from the region.

The *IRAS* luminosities of these sources, calculated from 7 to 135 μm using the method of Emerson (1987), are listed in column (13) of Table 5. These luminosities are within the range of less than $\sim 20 L_\odot$, with a mean value of $10.7 L_\odot$. The low luminosities of infrared sources in the region set an upper limit of masses of newly formed stars and indicate that young stellar objects formed from current clouds are generally of low-mass, solar-type stars.

The surface density of *IRAS* sources within the ^{13}CO cloud, 79 deg^{-2} , is 6 times of that outside the cloud, 13 deg^{-2} , as counted within the frame of Figure 1. This supports the fact that many of the sources inside the cloud boundary must be in real association with the cloud. Furthermore, the surface density of *IRAS* sources in the south cloud, 122 deg^{-2} , is more than twice that of the north cloud. This difference cannot be simply due to statistical fluctuation. Instead, it may reflect the difference of star-forming efficiencies between the two clouds. If so, the south cloud should be more consumed mass and devel-

oped in formation of stars than the north cloud. It seems reasonable that the column density of the south cloud is observed to be smaller than that of the north cloud (see Table 2) if the molecular material has been depleted more in the south cloud than in the north cloud during star formation. Considering the low star-forming efficiency of these clouds, the gas depletion is suggested mainly through dispersion instead of being bound into stellar masses.

b) Low-Mass Star Formation over the Galactic Scale

The existence of dense clouds at large distances and without significant optical indication can only be unambiguously revealed by detailed CO survey mapping. A large-scale survey of molecular clouds in the Galaxy shows that three-fourths of all molecular cores belong to the disk population of cold cloud cores with properties basically similar to those of dark clouds in the solar neighborhood (Solomon, Sanders, and Rivolo 1985). These cold cores are distributed somewhat randomly among arm and interarm regions. Clouds such as those studied here may serve as a link between nearby dark clouds and those cold cores revealed by large-scale surveys. The evidence for star formation in the current cloud may suggest that low-mass star formation is not only occurring in the solar neighborhood, but also in spiral arm or interarm regions, defined by the distribution of their parent clouds. There is no doubt that many such clouds are still missed by the observations. Extension of current studies of low-mass star formation to further distances will be promising for a better understanding of low-mass star formation over the Galactic scale.

VI. CONCLUSIONS

M120.1+3.0, a dense and filamentary molecular cloud, has been discovered in the Cep OB4 region from a large-scale ^{13}CO survey. Detailed studies have been made of the cloud. Molecular properties revealed from ^{13}CO suggest that the cloud is dense and massive ($M = 1500 M_\odot$). The *IRAS* sources are distributed in good coincidence with the dense gas distribution. All sources are low-luminosity objects ($L \lesssim 20 L_\odot$). The close association between infrared sources and dense molecular material suggests some of these sources are embedded inside the dense molecular material. Two molecular outflows have been discovered in this region. They provide convincing evidence of star formation in this cloud. Present study provides a good example of a low-mass star-forming region with a distance of more than 500 pc. The combination of present observations and large-scale surveys suggests the general existence of low-mass star-forming clouds. Detailed studies will be helpful to understand low-mass star formation over the Galactic scales.

The authors are grateful to A. Mizuno for his patience in maintaining the 4 m telescope during observations. It is the authors' pleasure to thank staffs at IPAC for their kind help in reducing the co-added data. Thanks are due to K. Tatematsu for his careful reading of the manuscript. One of the authors, Y. J., wishes to express his sincere thanks to Inoue Foundation of Japan for financial aid. He also wishes to express thanks to K. Kawabata and S. Nozawa for their help during the molecular-line observation and data reduction. This work is financially supported by the Grant-in-Aid for Science Research of the Ministry of Education, Science, and Culture, Japan (Nos. 62420002, 63611511, and 01065002).

REFERENCES

- Beichman, C. A. 1986, in *Light on Dark Matter*, ed. F. P. Israel (Dordrecht: Reidel), p. 279.
- Beichman, C. A., Myers, P. C., Emerson, J. P., Harris, S., Mathieu, R., Benson, P. J., and Jennings, R. E. 1986, *Ap. J.*, **307**, 337.
- Dame, T. M., Ungerechts, H., Cohen, R. S., de Gues, E. J., Grenier, I. A., May, J., Murphy, D. C., Nyman, L.-Å., and Thaddeus, P. 1987, *Ap. J.*, **322**, 706.
- Dickman, R. L. 1978, *Ap. J. Suppl.*, **37**, 407.
- Edwards, S., and Snell, R. L. 1984, *Ap. J.*, **281**, 237.
- Emerson, J. P. 1987, in *Formation and Evolution of Low Mass Stars*, ed. A. K. Dupree and M. T. V. L. Lago (Dordrecht: Kluwer), p. 193.
- Frerking, M., and Langer, W. 1982, *Ap. J.*, **256**, 523.
- Fukui, Y. 1988, *Vistas Astr.*, **31**, 217.
- . 1989, in *Proc. ESO Workshop on Low-Mass Star Formation and Pre-Main Sequence Objects*, ed. B. Reipurth (Garching: ESO), p. 95.
- Fukui, Y., Iwata, T., Mizuno, A., Bally, J., and Lane, A. P. 1990, in *Protostars and Planets III* (Tucson: University of Arizona Press), in press.
- Fukui, Y., Iwata, T., Takaba, H., Mizuno, A., Ogawa, H., Kawabata, K., and Sugitani, K. 1989, *Nature*, **342**, 161.
- Fukui, Y., Sugitani, K., Takaba, H., Iwata, T., Mozuno, A., Ogawa, H., and Kawabata, K. 1986, *Ap. J. (Letters)*, **311**, L85.
- Goldsmith, P. F., and Arquilla, R. 1985, in *Protostars and Planets II*, ed. D. C. Black and M. S. Matthews (Tucson: University of Arizona Press), p. 301.
- Goldsmith, P. F., Snell, R. L., Hemeon-Heyer, M., and Langer, W. D. 1984, *Ap. J.*, **286**, 599.
- Herbst, W., and Sawyer, D. L. 1981, *Ap. J.*, **243**, 935.
- IRAS Point Source Catalog*. 1988, Joint IRAS Science Working Group (Washington, DC: US GPO).
- Kawabata, K., Ogawa, H., Fukui, Y., Takano, T., Fujimoto, Y., Kawabe, R., Sugitani, K., and Takaba, H. 1985, *Astr. Ap.*, **151**, 1.
- Langer, W. D., Wilson, R. W., Goldsmith, P. F., and Beichman, C. A. 1989, *Ap. J.*, **337**, 355.
- Lozinskaya, T. A., Sitnik, T. G., and Toropova, M. S. 1987, *Soviet Astr.*, **31**, 493.
- MacConnell, D. J. 1968, *Ap. J. Suppl.*, **16**, 275.
- Myers, P. C., Linke, R., and Benson, P. J. 1983, *Ap. J.*, **264**, 517.
- Phillips, J. P., White, G. J., Rainey, R., Avery, L. W., Richardson, K. J., Griffin, M. J., Cronin, N. J., Monteiro, T., and Hilton, J. 1988, *Astr. Ap.*, **190**, 289.
- Plambeck, R. L., Snell, R. L., and Loren, R. B. 1983, *Ap. J.*, **266**, 321.
- Snell, R. L., Scoville, N. Z., Sanders, D. B., and Erickson, N. R. 1984, *Ap. J.*, **284**, 176.
- Solomon, P. M., Sanders, D. B., and Rivolo, A. R. 1985, *Ap. J. (Letters)*, **292**, L19.
- Yang, J., and Fukui, Y. 1990, in preparation.
- Young, J. S., Goldsmith, P. F., Langer, W. D., Wilson, R. W., and Carlson, E. R. 1982, *Ap. J.*, **261**, 513.

HUA CHEN: Institute for Astronomy, University of Hawaii, 2680 Woodlawn Drive, Honolulu, HI 96822

YASUO FUKUI, HIDEO OGAWA, TOMOFUMI UMEMOTO, and JI YANG: Department of Astrophysics, Nagoya University, Chikusa-ku, Nagoya 464-01, Japan